European Journal of Pharmaceutics and Biopharmaceutics 73 (2009) 130–139

Contents lists available at ScienceDirect

European Journal of Pharmaceutics and Biopharmaceutics

journal homepage: www.elsevier.com/locate/ejpb

Research paper

Characterization and superficial transformations on mini-matrices made of interpolymer complexes of chitosan and carboxymethylcellulose during *in vitro* clarithromycin release

Marta Gómez-Burgaz [a], Guillermo Torrado [b], Santiago Torrado [a,*]

[a] Department of Pharmaceutical Technology, School of Pharmacy, Complutense University, Madrid, Spain
[b] Department of Pharmaceutical Technology, School of Pharmacy, Alcalá de Henares University, Madrid, Spain

ARTICLE INFO

Article history:
Received 15 September 2008
Accepted in revised form 17 April 2009
Available online 3 May 2009

Keywords:
Grazing incidence X-ray
Polymeric interactions
Clarithromycin
Chitosan
Sustained release

ABSTRACT

Different interpolymer complexes (IPCs) of chitosan (CS) and carboxymethylcellulose sodium salt (CMC) were used to elaborate mini-matrices containing clarithromycin (CAM). IPCs were characterized by FTIR, DSC and powder X-ray (XRD).

Compression processes did not modify the physical state of CAM which was in its polymorph Form II. However, during tableting, polymer/polymer interactions occurred to form matrix systems that were confirmed by DSC.

When mini-matrices were placed in acetate buffer (pH 4.2), the formation of a CAM solvate was determined by XRD, FTIR and DSC, showing the presence of incorporated crystallizing solvent molecules. Grazing incidence X-ray diffraction (GID) enabled us to profile transformations of CAM on surfaces of mini-matrices when it is in intimate contact with dissolution medium, and its conversion to a solvate form prior to its dissolution process. Besides, FTIR and DSC revealed polymer–polymer electrostatic interactions during dissolution process.

Furthermore, swelling and eroding studies and *in vitro* drug release exhibited that when increasing the amount of CS within IPCs, swelling and erosion rates were greater and CAM release was faster. Zero-order kinetics from drug release profiles were related to linear erosion kinetics, and highlighted that erosion played an important role in drug release due to CAM poor solubility at this pH.

1. Introduction

Clarithromycin (CAM) (6-O-methylerithromycin) is a semi-synthetic, orally absorbed and broad-spectrum antibiotic. It has been reported that CAM has at least four distinct crystalline forms: "Form 0", "Form I", "Form II" and "Form IV". These polymorphs have been identified as indicated in US Pat. No. 5,945,405 and the patents WO/1998/004573, WO/1998/004574 and WO/2001/044262 [1–4]. The crystal forms and/or solvates of CAM can be typically identified by powder X-ray diffraction, and they may have different thermal stability, dissolution characteristics and bioavailability. Form II, which is more stable than Form I, is used in the drug formulation currently on the market. Both forms have an identical spectrum of antibacterial activity, but Form I crystals unexpectedly have an intrinsic rate of dissolution about three times that of Form II crystals [3]. The Form 0 is a solvate having an incorporated crystallizing solvent molecule, and its X-ray pattern may be somewhat varied depending on the solvent [1].

The clinical efficacy of CAM has been confirmed in the clearance of lower and upper respiratory tract infections and in the treatment of *Helicobacter pylori*, which is a causative agent in chronic active gastritis, gastric and duodenal ulcers, and gastric adenocarcinoma [5]. *Helicobacter pylori* is susceptible to many antibiotics *in vitro*, but has proved difficult to eradicate *in vivo* [6]. The reasons for this incomplete eradication are the gastric location of the pathogen, the degradation of some antibiotics like erythromycin and CAM in acidic conditions [7] and the gastrointestinal side effects associated with CAM, like gastric discomfort, abnormal taste and diarrhoea [8].

It is believed that the administration of CAM in intragastric controlled-release devices using mucoadhesive and swellable polymers, like chitosan, alginates or celluloses, could have a double advantage in these therapies. First, it could improve patient compliance by improving its therapeutic effect and reducing its dose-related side effects [8]. Secondly, it can have high clearance due to their ability to increase the contact time of the drug with the biological substrate, thus increasing drug absorption and allowing it to diffuse through the intracellular localization of *H. pylori* [9].

* Corresponding author. Departamento de Farmacia y Tecnología Farmacéutica, Facultad de Farmacia, Universidad Complutense de Madrid., Avda, Complutense s/n, 28040 Madrid, Spain. Tel.: +34 91 394 17 27; fax: +34 91 394 17 36.
E-mail address: torrado2@farm.ucm.es (S. Torrado).

0939-6411/$ - see front matter © 2009 Elsevier B.V. All rights reserved.
doi:10.1016/j.ejpb.2009.04.004

Chitosan (CS) (β-(1–4)-2-amino-2-deoxy-D-glucose) is a linear hydrophilic polysaccharide polymer of D-glucosamine and can be prepared by the N-deacetylation of chitin. This natural polysaccharide possesses useful properties such as non-toxicity, high biocompatibility and non-antigenicity. Also, CS is mucoadhesive and enhances the penetration of drugs across the intestinal and nasal barriers. In neutral or basic pH conditions, CS contains free amino groups and hence, it is insoluble in water. In acidic conditions, amino groups can undergo protonation, thus, making it soluble in water [10]. Carboxymethylcellulose (CMC) is a semi-synthetic derivative of cellulose. It is a water-soluble linear polymer, produced by partial substitution of the 2, 3 and 6 hydroxymethyl groups of cellulose by hydrophobic carboxymethyl groups. CMC chains are linear (1 → 4)-linked glycanes, whose polyelectrolyte character is due to the presence of weakly acidic groups. At pH level above 4, it behaves as a polyanion. The average degree of substitution (α) of CMC is defined as the average numbers of carboxymethyl groups per repeating unit. It is generally found in a water-soluble form as sodium salt [11].

Recently, interpolymer complexes (IPCs) have attracted considerable interest by pharmaceutical researchers on account of its unique characteristics due to a specific interaction between constituent polymers such as hydrogen bonds, electrostatic interactions, van der Waals forces or hydrophobic interactions. Previous studies have reported the formation of IPCs between the protonated amine groups of CS, as the polycationic polymer, and the carboxylate groups of polyanionic polymer such as hyaluronate sodium [12], poly(acrylic acid) [13], alginate [14] or xanthans [15]. In a similar manner, it may be expected that IPC will be formed among carboxylic groups from CMC and amino moieties from CS, as a result of the advance of dissolution medium front within mini-matrices.

The purposes of this study were to: (i) characterize interpolymer complexes of CS and CMC and (ii) study the physical state of CAM by grazing incidence X-ray diffraction (GID) as a method for profiling transformations occurred on the surfaces of matrices prepared with these interpolymer complexes.

2. Materials and methods

2.1. Materials

High viscous Chitosan (CS; 1406 mPa s) was purchased from Sigma–Aldrich (Spain), with a minimum degree of acetylation of 75%. Carboxymethylcellulose (CMC) sodium salt (high viscosity, range from 1500 to 2500 mPa s) was supplied by BDS (Lutterworth, UK), and clarithromycin (CAM) was provided by Normon (Spain). All other chemicals were of pharmaceutical grade or better and used without further purification.

2.2. Preparation of drug delivery systems

The novel method called "tablets-in-capsule system" [16] is based on the combination of different mini-tablets to obtain drug delivery systems. Following this method, we prepared different formulations that consisted of mini-matrices (6 mm in diameter) inside a hard gelatine capsule.

To study the relation of polymer/polymer within the network, hydrogels in the ratio of CAM:[CS:CMC] 80:[20] (w/w) were prepared, where the proportions of [CS:CMC] were 0:100, 25:75, 50:50, 75:25, 90:10 and 100:0 (w/w), henceforth designated as 80:[0:100], 80:[25:75], 80:[50:50], 80:[75:25], 80:[90:10] and 80:[0:100].

The systems were prepared as follow. First, drug and polymers were sieved through 0.45-mm mesh and then mixed homogeneously. Afterwards, they were directly compressed to get mini-matrices of 6 mm in diameter and weight of 50 mg. Ten of these mini-matrices were placed into a gelatine capsule, and they constituted the final system.

2.3. Powder and grazing incidence X-ray diffraction (GID)

Powder X-ray diffraction patterns of pure polymers (CS and CMC) and drug (CAM) were measured using powder X-ray diffractometer (Philips X'Pert SW, CAI, UCM) with Ni-filtered CuKα radiation generated at 30 kV and 30 mA as an X-ray source.

GID is a technique in which the incident angle (θ) remains fixed as the detector turns normally around the axis of the goniometer [17]. GID measurements were performed with a laboratory X-ray diffractometer, model Philips X'Pert SW, and the radiation was the same as the powder measurements. In this study, we used an incident angle (θ) of 1°. Prior to the measurements, the instrument was aligned and calibrated carefully. A special, height-adjustable, tablet-sample holder was used for the measurements.

At these conditions, we measured samples of mini-matrices at initial time (after tableting) and mini-matrices during the dissolution test at predetermined times points (1, 2, 4 and 6 h) that were withdrawn from the dissolution medium and lyophilized.

In order to calculate the penetration depth, elemental analysis measurements were performed in matrices with an elemental analyzer LECO CHNS-932. The N, C and H contents were determined directly, while the O content was calculated from the difference between unity and the percentage sum of N, C and H contents. The composition of matrices was used to determine the mass absorption coefficients (MAC) with the help of mass-absorption-calculator (X'Pert HighScore). This calculator uses the mass absorption coefficients (μ/ρ) and the atomic weights of the elements. First, the molecular weight, the atomic weight fractions (W_n) and the mass absorption coefficient (μ/ρ) of a compound are calculated as follows:

$$\mu/\rho_{compound} = W_1 \times (\mu/\rho)_1 + W_2 \times (\mu/\rho)_2 + \cdots + W_n \times (\mu/\rho)_n \quad (1)$$

And then, the penetration depth can be calculated from the MAC of the mixture and the real density. To determine the true density, a sample is weighted (M) and placed in the cell chamber cup of a multivolume pycnometer (1305, Micrometrics) to measure the true volume (V_t). The true density (ρ_t) was then calculated.

Firstly, the path length (L) is calculated with the formula:

$$I_L = I_0 \exp^{-(\mu/\rho)\rho_t L} \quad (2)$$

This is the length the X-rays travel through the sample, until 99% of the intensity (I_L) is absorbed, and only 1% of the initial intensity (I_0) is transmitted.

Next, the penetration depth (τ) is established with the simplified formula, which is only correct for symmetric case (gonio scans):

$$\tau = 0.5 L \sin(\theta) \quad (3)$$

The penetration depth is the thickness of the sample, contributing 99% of the diffracted intensity for a given incident angle θ.

2.4. Characterization of CS–CMC complexes via infra-red spectroscopy (FTIR)

A Nicolet model Magna 750 Series II infra-red spectrometer was used. The scan range was 500–4000 cm^{-1}. Each spectrum was automatically averaged over 16 scans obtained at a spectral resolution of 4 cm^{-1}.

We measured samples of mini-matrices at initial time (after tableting) and mini-matrices during the dissolution test at predetermined times points (1, 2, 4 and 6 h) that were withdrawn from

the dissolution medium and lyophilized. Then, these samples were thoroughly ground with exhaustively dried KBr, and pellets were prepared by compression under vacuum. A sample cup filled with dried KBr powder was used as the background data set.

2.5. Characterization of CS–CMC complexes via differential scanning calorimetry (DSC)

Differential scanning calorimetric (DSC) analysis was used to characterize the thermal behaviour of the individual polymers, CAM and complexes CS–CMC.

DSC thermograms were obtained using an automatic thermal analyzer system (Mettler Toledo TC 15, TA controller). Temperature calibration was performed using Indium Calibration Reference Standard (transition point 156.60 °C).

We measured samples of mini-matrices at initial time (after tableting) and mini-matrices during the dissolution test at predetermined times points (1, 2 and 6 h) that were withdrawn from the dissolution medium and lyophilized. Then, these samples were crimped in standard aluminium pans and heated from 25 to 350 °C at a heating rate of 10 °C/min under constant purging of dry nitrogen 30 mL/min. An empty pan, sealed in the same way as the sample, was used as a reference.

2.6. In vitro drug release

These studies were carried out in a dissolution bath (Vankel VK 700). A USP Apparatus 2 (paddle) was set up at 37 °C, with a rotational speed of 50 rpm, and 500 mL of dissolution medium were added to each vessel.

The final system (capsule with 10 mini-matrices) was weighed and placed in each vessel. At predetermined times points, a sample of 5 mL was withdrawn. Before analysing any sample, they were filtered through a 0.45-μm filter (Acrodisc® HPVL 0.45 μm).

The quantity of CAM, at each time, was determined by HPLC method, consisting of a UV detector (Jasco UV-1575 Intelligent UV/VIS Detector), a pump (Jasco PU-1580 Intelligent HPLC pump), an automatic injector (Gilson 231 XL Sampling Injector) and a dilutor (Gilson 410 Dilutor). The selected wavelength was 210 nm. A C18 column was used (ACE® 5 C18), a 4.6-mm × 15-cm column with a particle size of 5 μm, and temperature was maintained constant at approximately 60 °C (Pickering Laboratories CHX700 Column Temperature Controller). The flow rate was 1.0 mL/min. The mobile phase consisted of a mixture of methanol and 0.079 M monobasic potassium phosphate (650:350), and the pH level was adjusted to 4.5 with phosphoric acid. The cumulative amount of CAM released from the system was determined from the appropriated calibration curve. Each determination at each time point was performed in triplicate, and the error bars on the graphs represented the standard deviation.

The dissolution media tested were acetate buffer (pH 4.2) prepared as described in USP 30 – NF 25 (2007) due to the use of proton pump inhibitors (PPIs) in the eradication therapies as gastric protectors which arise the pH level to a 24-h median of 4.2 [18].

2.7. Swelling and eroding studies

The method used was based on the studies of Kavanagh and Corrigan [19]. A USP Apparatus 2 (paddle) dissolution bath (Vankel VK 700) was used set to 37 °C. The rotational speed was 50 rpm, 250 mL of dissolution medium were measured and loaded into each of the six vessels of the dissolution bath and allowed to equilibrate before starting the experiment. Each system (capsule with mini-matrices) was weighed (W_i) and placed in each vessel. The experiment consisted of allowing the system to dissolve in the media at the listed conditions for certain time periods. After vacuum filtration, to drain the excess of medium, the remaining system was weighted to determine its wet weight (W_w). The system was then dried in an oven at 37 °C to measure constant weight (W_d). Each determination at each point was carried out in triplicate, and the error bars on the graphs represented the standard deviation.

The swelling and erosion ratios were measured at two different conditions: (i) in a pH level range from 1.2 to 7.2 at 2 h, using buffer solutions as indicated by USP 30 – NF 25 (2007) and (ii) in a time range from 15 min to 6 h at a buffer solution of pH 4.2.

The indicators calculated were, firstly, the relative swelling which is calculated as follows [19]:

$$Relative\ Swelling = \frac{W_w}{W_i} \tag{4}$$

To investigate more precisely the relative swelling mechanism into hydrophilic matrices, the initial swelling data were analysed according to the following equation for $W_t/W_\infty < 0.6$ [20]:

$$\frac{W_t}{W_\infty} = K_S t^n \tag{5}$$

where K_S (h^{-1}) is a characteristic constant of the hydrogel, and n is a characteristic exponent related to the mode of transport of the penetrant.

Data of dry weight are used to calculate the relative erosion indicator. This index is calculated as an indicator of the erosion and dissolution of the system.

$$Relative\ Erosion = \frac{W_d}{W_i} \tag{6}$$

These values were fitted to the cube root relationship as outlined by Kavanagh and Corrigan [19] to determine the apparent polymer erosion rate constant (K_d).

$$(Wd/Wi)^{\frac{1}{3}} = 1 - K_d t \tag{7}$$

All statistics were obtained with Statgraphics® Plus, version 5.1.

3. Results and discussion

3.1. Grazing and powder X-ray studies

The commonly used techniques for physical characterization are X-ray powder diffractometry (XRD), differential scanning calorimetry (DSC), infra-red spectroscopy (IR) and scanning electron microscopy (SEM). Because the medium is in intimate contact with the surface of the matrices and transformations of the dissolving particle will take place near the surface, the use of other techniques such as grazing incident X-ray diffractometry (GID) will permit to evaluate these conversions [21].

Fig. 1 shows the comparison between XRD and GID patterns of different tablets containing CAM. The classical XRD patterns (Fig. 1A) did not depict any characteristic peak of CAM; hence this technique was not useful to characterize the physical state of the CAM within IPC. However, when using GID (Fig. 1B), it was possible to distinguish the characteristic peaks of CAM, revealing that this technique is appropriate to study the physical state of drugs entrapped within IPCs. Furthermore, one advantage of this technique is the possibility to modify the incidence angle, and in consequence different penetration depths and patterns will be obtained [21]. Studies with different incidence angles, ranging from 0.1° to 10°, were carried out (data not shown), and the patterns obtained from these studies were similar in all cases. The penetration depths calculated, according to the composition and the density of tablets, ranged from 9 to 950 μm. The similarity of the patterns can be explained by the penetration depths, which were not deep enough to

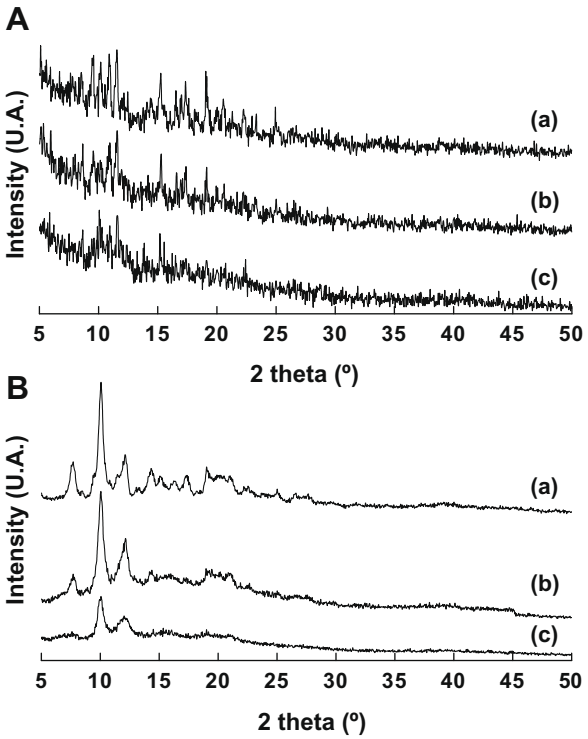

Fig. 1. Comparison between powder X-ray diffraction (XRD) (A) and grazing X-ray diffraction (GID) (B) patterns of CAM:[CS:CMC] (w/w) 80:[90:10] (a), 80:[50:50] (b) and 80:[0:100] (c) in acetate buffer (pH 4.2) at 37 °C and at 1 h.

get to the layer where no dissolution medium had imbibed. Since all patterns were similar at different incidence angles, we selected the angle of 1° to characterize the physical state of CAM during *in vitro* release studies. This angle is commonly used by other authors utilizing this technique [17,21].

Penetration depths were confirmed by photographs of the tablets at different times (Fig. 2). The dissolution medium advanced through the matrices forming gel layers, as it can be observed. A gel layer larger than 1.5 mm from 1 h is observed in all the systems. According to these photographs, it is possible to expect a greater swelling from CAM:[CS:CMC] 80:[90:10] (w/w) (Fig. 2A) compare to CAM:[CS:CMC] 80:[50:50] (Fig. 2B) and 80:[0:100] (Fig. 2C) (w/w). This fact was confirmed with swelling and eroding studies, and will be discussed in more detail in the later sections.

Fig. 3a and b shows XRD patterns of intact CAM and CAM when it is placed into acetate buffer. These patterns depict that intact CAM is the crystal Form II of CAM which is characterized by 2-θ angle position at 8.5° ± 0.2, 9.5° ± 0.2, 10.8° ± 0.2 and 11.5° ± 0.2 [4,22]. However, when CAM is placed in acetate buffer (pH 4.2), a different XRD pattern is obtained with characteristic peaks at 2θ = 10.06° ± 0.2 and 12.14° ± 0.2. These differences between XRD patterns can be attributed to the formation of a solvate form that does not correspond with the described forms of CAM Form I and Form IV [22,23].

The XRD patterns from intact CMC and CS and after placing in acetate buffer are depicted in Fig. 3c–f. The diffractogram of CMC raw material showed that it was mostly amorphous (Fig. 3c), while pure CS was shown to be almost a halo pattern (Fig. 3e). It can be noted that CS powder was of semicrystalline state. This material had a modest degree of crystallinity depending on the partial acylation. Similar crystallinity results had been reported previously by Ghaffari et al. [24]. Nevertheless, in Fig. 3d and f, both polymers exhibited the typical pattern of an amorphous product when placed in acetate buffer [25].

Changes in the surface of matrices, due to intimate contact with the dissolution medium, were studied by GID and are shown in Fig. 4. When IPCs are placed in acetate buffer (pH 4.2), CAM "Form II" is converted to a solvate form of CAM. This is demonstrated by the presence of the characteristic peaks at 2θ = 10.06° ± 0.2 and 12.14° ± 0.2.

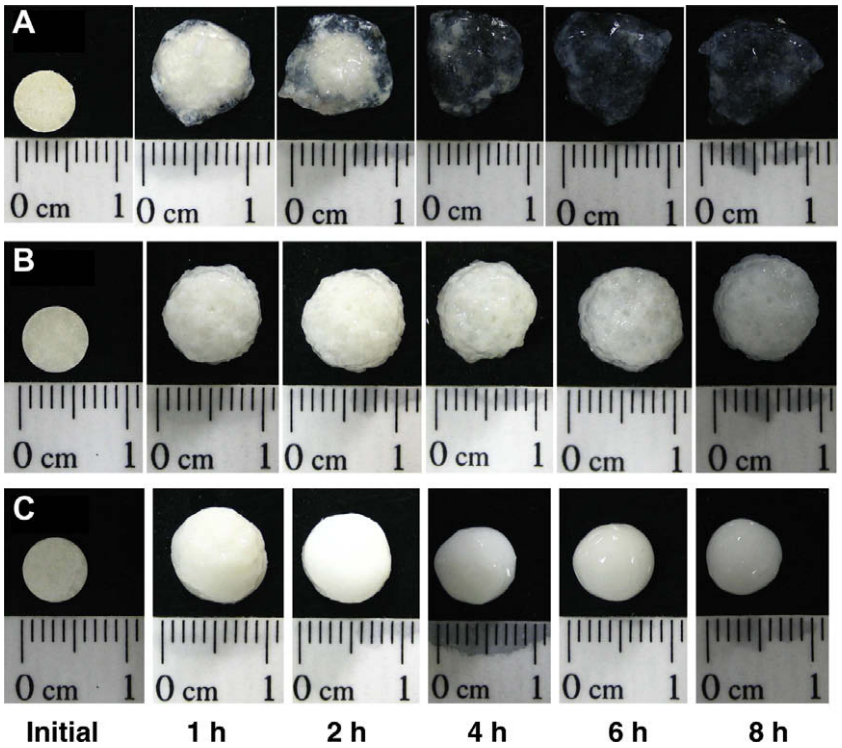

Fig. 2. Photographs of matrices CAM:[CS:CMC] (w/w) 80:[90:10] (A), 80:[50:50] (B) and 80:[0:100] (C) in acetate buffer (pH 4.2) at 37 °C.

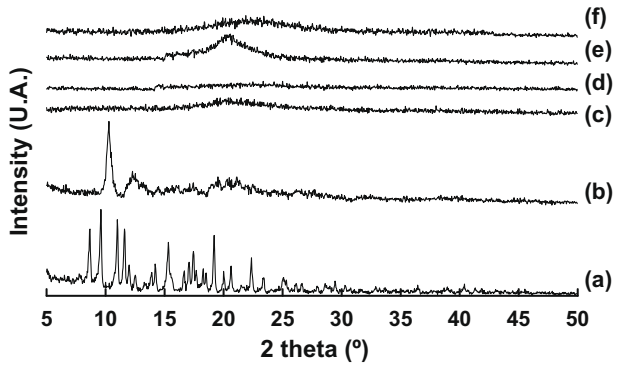

Fig. 3. Powder X-ray diffraction (XRD) patterns of CAM: raw material (a) and in acetate buffer (b). XRD patterns of CMC: raw material (c) and in acetate buffer (d). XRD patterns of CS: raw material (e) and in acetate buffer (f).

A decrease in the intensity of characteristic X-ray diffraction peak (10.06° (2θ)) of the solvate was found with increasing in time into acetate buffer. The tendency followed a linear behaviour in all cases ($r^2 > 0.938$). This can be explained by a less content of CAM, in its solvate form, remained within IPCs. Thus, in all the studied formulation, the mixture of polymers (CS–CMC) imbibed the dissolution medium forming a hydrogel layer, due to the ionization of their moieties, where CAM "Form II" is transformed into its solvate form prior to its dissolution step.

Combining these solid phase measurements with the drug released profiles can offer a deeper understanding of the medium-mediated phase transformation phenomena on surfaces during dissolution processes [26].

3.2. FTIR

To obtain information regarding the molecular structure of the swollen CS:CMC IPCs, the FTIR spectra from these complexes at different times were obtained after swelling in acetate buffer (pH 4.2). The spectra are shown in Figs. 5 and 6.

The characteristic peaks of CAM (Fig. 5a and b) are about 1695 and 1733 cm^{-1} that are attributed to $\nu_{C=O}$ stretching vibration from ketone group in a lactone ring and to $\nu_{O-C=O}$ stretching vibration in a lactone ring [22]. However, when CAM was placed in acetate buffer, a solvation process took placed, and a solvate of CAM was formed. Other solvate forms have been reported previously in different drugs [27–29]. They were defined as a solvate having an incorporated crystallizing solvent molecule, and its X-ray pattern and FTIR spectrum may be somewhat varied depending on the solvent [1]. The presence of two new peaks at 1413 and 1565 cm^{-1}, which were assigned to the vibration of symmetric and asymmetric carboxylic groups [30], demonstrated the presence of crystal from the solvent, and consistently the formation of the solvate.

In the CS spectrum (Fig. 5c and d), peaks at 1630 and 1365 cm^{-1} were characteristic peaks of amide groups: amide I and amide III, respectively. When CS was placed in acetate buffer, its spectrum showed a peak at 1674 cm^{-1} that was attributed to the formation of tertiary amide ($-NH_3^+$) [13]. The CMC spectrum (Fig. 5e and f) presented two strong peaks at 1620 and 1434 cm^{-1} that were assigned to the asymmetric and symmetric carboxylate vibration, respectively [31]. The fact that in acetate buffer (pH 4.2) these peaks were more marked was attributed to the formation of the polyion in this condition.

Regarding the characterization of CAM within IPCs, the spectra at initial time (Fig. 6A(a), B(a) and C(a)) were similar to the one of CAM raw material (Fig. 5a). This is an indication of non-interaction between CAM and polymers. Similar results were observed by other authors within polyionic complexes and drugs with carbox-

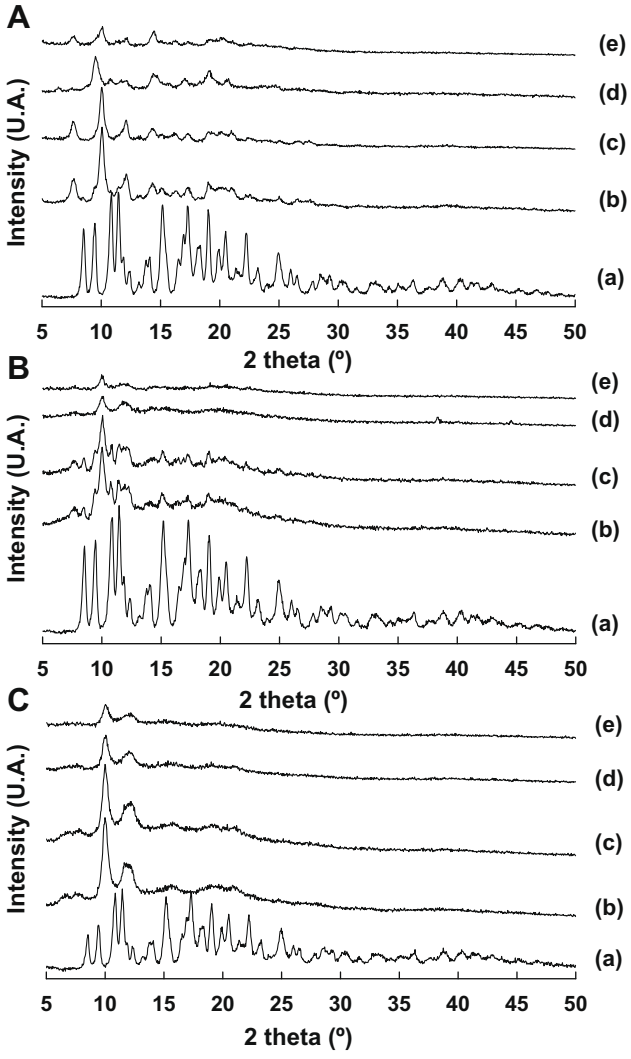

Fig. 4. Grazing X-ray diffraction (GID) patterns of CAM:[CS:CMC] (w/w) 80:[90:10] (A), 80:[50:50] (B) and 80:[0:100] (C) in acetate buffer (pH 4.2) at 37 °C and at initial time (no exposure to dissolution medium) (a), 1 h (b), 2 h (c), 4 h (d) and 6 h (e). The incident angle is 1° in all cases.

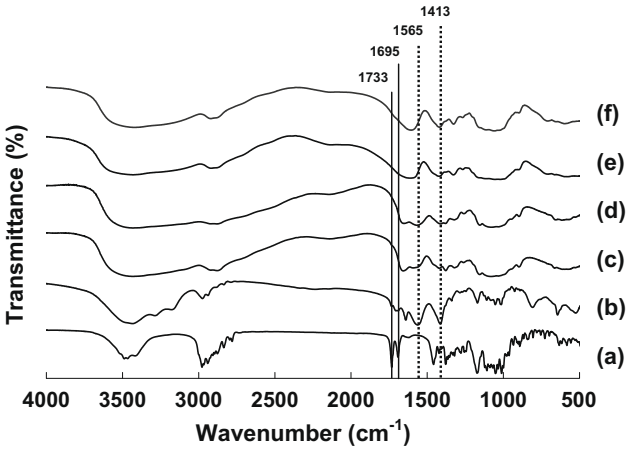

Fig. 5. FTIR spectra of CAM: raw material (a) and in acetate buffer (b). FTIR spectra of CMC: raw material (c) and in acetate buffer (d). FTIR spectra of CS: raw material (e) and in acetate buffer (f).

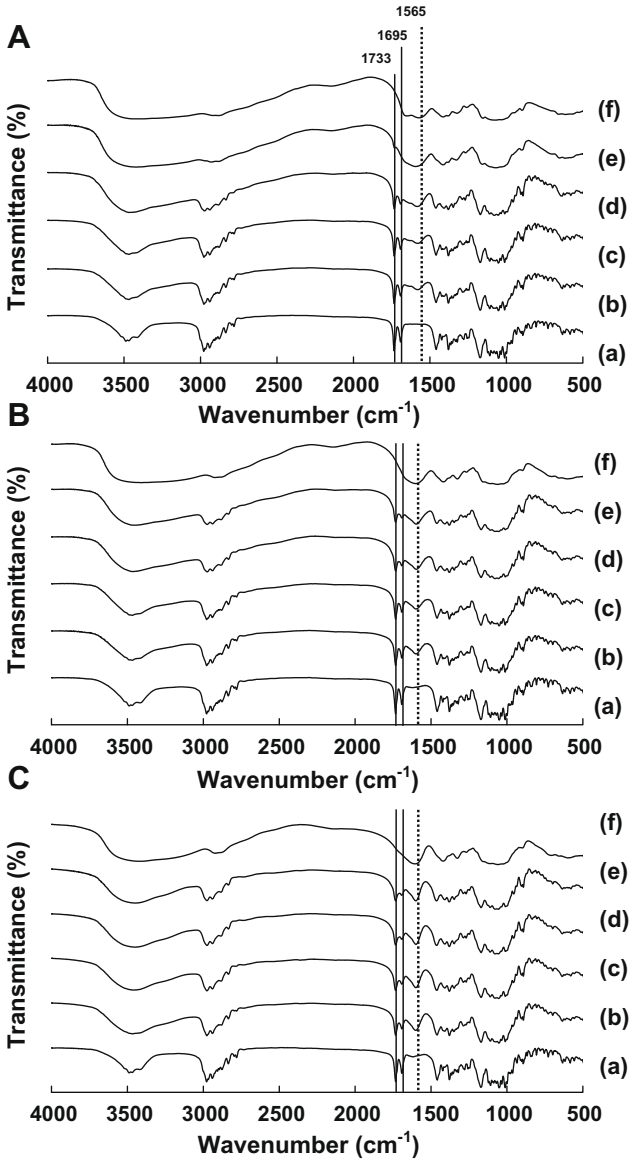

Fig. 6. FTIR spectra of CAM:[CS:CMC] 80:[90:10] (A), 80:[50:50] (B) and 80:[0:100] (C) (w/w) in acetate buffer (pH 4.2) at 37 °C and at initial time (no exposure to dissolution medium) (a), 1 h (b), 2 h (c), 4 h (d) and 6 h (e). Spectrum of IPC [CS:CMC] (w/w) without entrapped CAM and in acetate buffer (f).

ylic groups like amoxicillin [13]. The formation of solvates of CAM could be observed as a consequence of the entrance of the acetate buffer within the network (Fig. 6A (b–e), B (b–e) and C (b–e)), which was demonstrated with an increasing peak at 1565 cm^{-1} that is attributed to carboxylic groups from the medium. In these figures, other characteristic peaks of CAM were less defined meaning that less content of drug was remained within the network. This physical state of CAM could be observed in all spectra, with the exception of 80:[90:10] (w/w) at 6 h (Fig. 6A(e)), which spectrum was very similar to the IPCs without entrapped drug (Fig. 6A(f)).

However, it was difficult to distinguish interactions when comparing binary mixtures of both polymers due to the overlapping bands of CS and CMC at the same region, thus, it is not possible to suggest from FTIR spectra that hydrogen bonds and/or electrostatic interactions between carboxylic groups from CMC and amino moieties from CS were involved in the formation of IPCs made of CS and CMC.

3.3. DSC studies

Figs. 7 and 8 show the DSC thermograms of CAM, CS, CMC and IPCs in an initial form and after placed in acetate buffer (pH 4.2).

The DSC thermogram of acetate salts from lyophilized dissolution medium is depicted in Fig. 7a. and exhibited two endothermic characteristic peaks at 58 and 330 °C. The DSC thermogram of CAM raw material (Fig. 7b) corresponds, as expected, to the thermogram of the polymorph "Form II" that can be justified by the presence of an endothermic peak at 227 °C attributed to the melting process and followed by another endothermic peak at 295 °C, which is attributed to the decomposition process [23]. However, when CAM was in contact with acetate buffer since initial times, solvation processes took placed (Fig. 7c and d). These new CAM solvates exhibited two endothermic peaks at 58 and 320 °C attributed to acetate salts and two endothermic peaks at 225 and 255 °C from CAM. Considerable shifts of the endothermic peak temperature of acetate salts (from 330 to 320 °C) and of the decomposition of CAM (from 295 to 255 °C) were observed and are related to the incorporation of molecules of acetate within CAM molecular structure. Similar changes in DSC parameters were observed with different solvents, like ethanol, where CAM incorporated crystallizing solvent molecules obtaining "Form 0" [1].

The DSC thermograms of CS and CMC raw material are depicted in Fig. 7e and f, respectively. CS exhibited an endothermic peak at 165 °C, and an exothermic peak attributable to its decomposition appeared approximately at 320 °C [32,33]. While CMC had an endothermic peak at 190 °C, followed by an exothermic peak at 285 °C assigned to its decomposition.

Analysing the physical state of CAM at initial time from thermograms of IPCs (Fig. 8A(a), B(a) and C(a)), it is possible to observe that there were no changes in the crystallinity of the drug during the formulation process, which is justified by the presence of the characteristic peak of CAM at 228 °C. Similar results were obtained by other authors when studying other model drugs [34,35]. The lack of significant shifts of the melting endothermic peaks of CAM also revealed no evidence of solid-state interaction between drug and polymers after tableting process over the whole composition range and conditions studied. Same results were obtained from FTIR and X-ray studies.

Nevertheless, changes in the DSC thermal parameters from polymers have been observed. In the formulation CAM:[CS:CMC] 80:[90:10] (w/w) at initial time (Fig. 8A(a)), the endothermic peak of CS showed a drop in the temperature of its fusion peak from 165 to 158 °C, meanwhile the endothermic peak of CMC increased from 190 to 201 °C. In a similar manner, changes in the temperature of

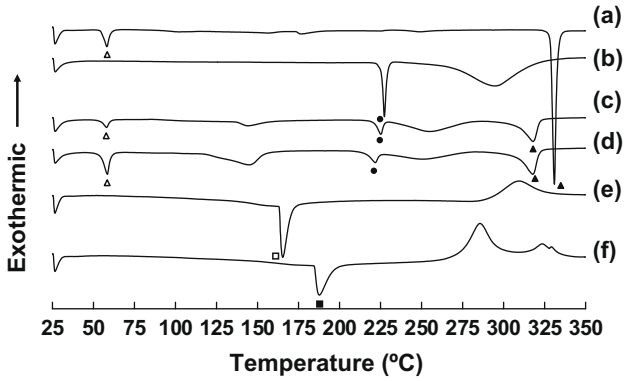

Fig. 7. DSC thermograms of lyophilized acetate buffer (a), CAM raw material (b), CAM in acetate buffer (pH 4.2), at 37 °C and at 1 h (c) and 6 h (d), CS raw material (e) and CMC raw material (f). Endothermic peaks of CAM (●), acetate salts (Δ, ▲), CS (□) and CMC (■).

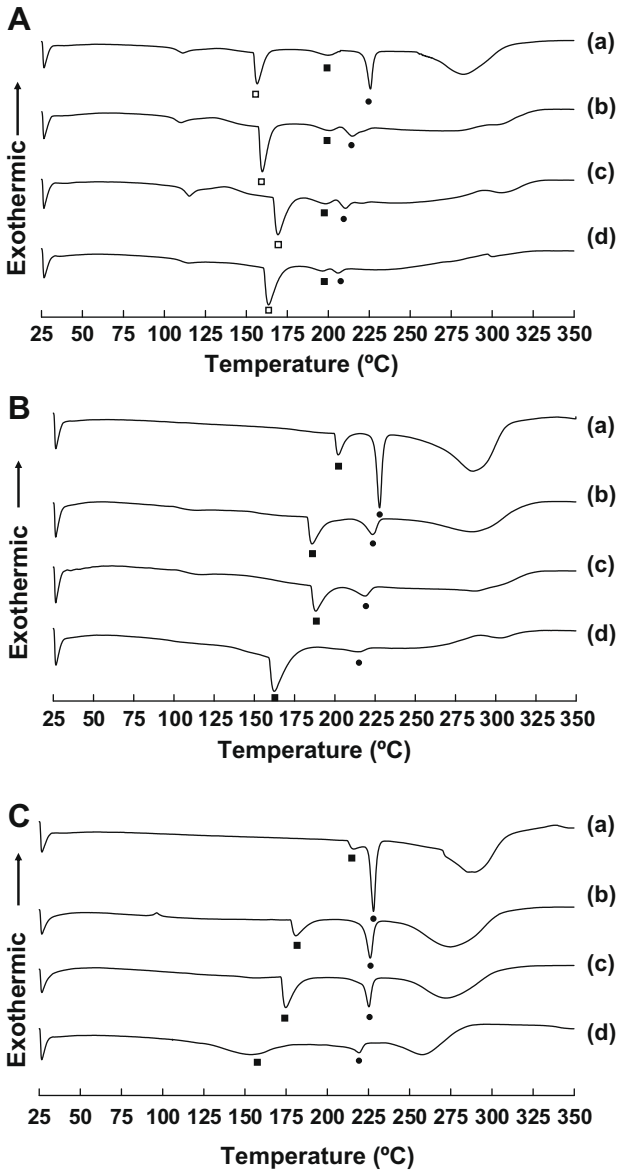

Fig. 8. DSC thermograms of CAM:[CS:CMC] (w/w) 80:[90:10] (A), 80:[50:50] (B) and 80:[0:100] (C) in acetate buffer (pH 4.2) at 37 °C and at initial time (no exposure to dissolution medium) (a), 1 h (b), 2 h (c) and 6 h (d). Endothermic peaks of CAM (●), CS (□) and CMC (■).

the endothermic peak of CMC appeared on the thermogram of CAM:[CS:CMC] 80:[50:50] (w/w) (Fig. 8B(a)) whose temperatures shifted until 199 °C, and CAM:[CS:CMC] 80:[0:100] (w/w) (Fig. 8C(a)) until 217 °C. These changes could be attributed to the formation of a matrix structure among polymeric chains from CS–CS, CS–CMC or CMC–CMC during the tableting processes, and these interactions were not possible to observe either with FTIR because of overlapping bands or with X-ray due to their amorphous nature. Unexpectedly, no peaks from CS were observed in the thermograms from CAM:[CS:CMC] 80:[50:50] (w/w), which could be explained by fewer CS ratios within the IPCs.

When complexes were placed in acetate buffer, some DSC events occurred. IPCs CAM:[CS:CMC] 80:[90:10] (w/w) (Fig. 8A(b–d)) showed thermal profiles with three endothermic peaks at about 158, 201 and 228 °C that were related to the characteristic peaks of CS, CMC and CAM, respectively. In Fig. 8A(b–d) and (B)b–d, it is possible to observe a decrease in the temperature of the endothermic peak of CAM, which ranges from 228 to 207 °C. This drop in the melting endothermic peak temperature could be related to the formation of the solvate form of CAM. However, in matrix systems comprised only CMC, CAM:[CS:CMC] 80:[0:100] (w/w) (Fig. 8C(b–d)), there was a fewer decrease in the temperature of the peak of CAM that only shifted from 228 to 220 °C. This fewer drop in the temperature could be related to the formation of the less amount of solvate of CAM within these systems. These findings allow us to expect a minor dissolution medium uptake per polymer remaining from these IPCs.

Furthermore, shifts on the endothermic peak temperatures of CMC and CS were addressed within CAM:[CS:CMC] 80:[90:10] (w/w) (Fig. 8A(b–d)). The peak of CS shifted from 165 to 158 °C, meanwhile the peak of CMC shifted from 188 to 200 °C. This could reveal the interactions among polymers due to the ionization processes of moieties from CS as a consequence of the advance of the solvent front. In a similar manner, changes in the endothermic peak temperatures of CMC were observed from CAM:[CS:CMC] 80:[50:50] (w/w) (Fig. 8C(b–d)) and CAM:[CS:CMC] 80:[0:100] (w/w) (Fig. 8C(b–d)), where the temperature, initially approximately at 190 °C, shifted until 156 °C due to the formation of hydrogen bonds at this pH levels.

3.4. Swelling and eroding properties

Since drug release from hydrogels is affected by the swelling and the rate of hydrogel degradation when exposed to gastric media, we studied both processes.

3.4.1. Influence of pH medium

CMC and CS are natural polyelectrolytes that have many carboxylic and amine moieties, respectively, in their molecular chains. The dissociation degree of these groups is closely related to the pH value of the medium. To investigate the influence of pH value of the medium on the swelling and eroding ratios, the pH range was selected from 1.2 to 7.2 for this study. As shown in Fig. 9A, IPCs have revealed to be pH dependent. All the studied systems showed an inflexion on their swelling behaviour at around 4.5–4.7 pH value which corresponds with the pK_a of carboxylic groups from CMC, approximately at 4.6 [36]. Below this pH value, IPCs that have greater swelling ratios are the ones with higher content of CS, meaning that carboxylic groups are protonated (–COOH) and the hydrogen bonds within IPCs can be formed. But at the same time, moieties from CS are also protonated ($-NH_3^+$), because the pH medium is below its pK_a 6.3 [37], causing repulsions that result in an increase in swelling.

On the contrary, for pH values above the pK_a of CS, IPCs that have greater swelling ratios are the ones with higher content of CMC. The carboxylic groups become ionized, thus the hydrogen bonding interactions are weakened and destroyed, as a result, the electrostatic repulsive force among the charge sites ($-COO^-$) causes an increasing in the swelling ratios when these groups are in higher densities.

Finally, for pH values between pK_a of polymers which range from 4.6 (CMC) to 6.3 (CS), the moieties from polymers become ionized having groups $-COO^-$ and $-NH_3^+$ within the network that created interactions between the oppositely charged moieties in CS and CMC, which have decreased the degree of swelling. However, it is important to highlight that IPCs with higher content of CMC showed an increased swelling ratio.

The erosion profiles are shown in Fig. 9B. In all cases, an increasing in eroding was related with an increase in relative swelling, which can be explained by hydrogen bonding and ionization of moieties from CS and CMC at different pH values that were related with their pK_a values.

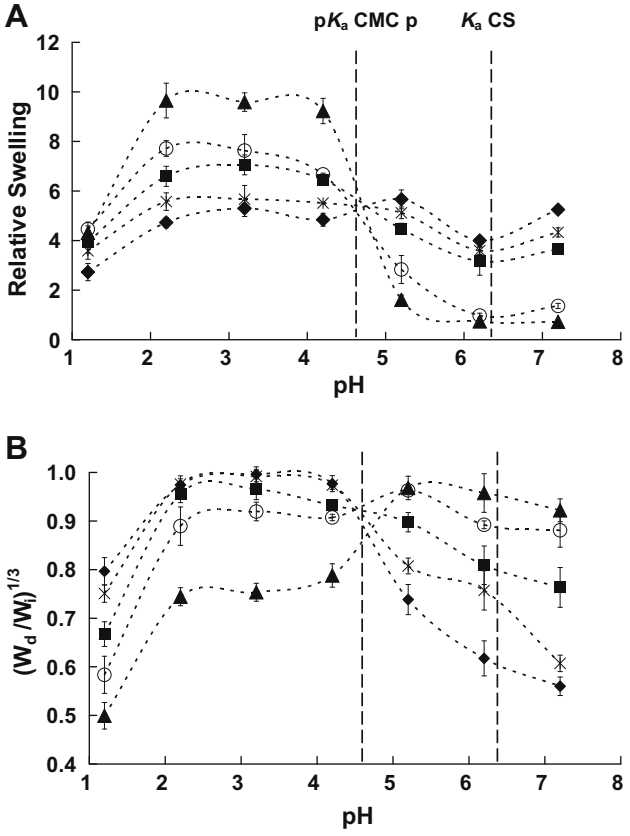

Fig. 9. *In vitro* relative swelling (A) and erosion kinetics (B) at 37 °C and at 2 h in a pH level range from 1.2 to 6.2 of CAM:[CS:CMC] (w/w) 80:[90:10] (▲), 80:[75:25] (○), 80:[50:50] (■), 80:[25:75] (∗) and 80:[0:100] (♦), $n = 3$.

3.4.2. Influence of CS and CMC within IPCs

Fig. 10A reports the relative swelling of IPCs with different proportions of CS:CMC (w/w). In terms of relative swelling, the graphs showed higher relative swelling for complexes with higher CS ratio, such as 80:[90:10], with a maximum relative swelling of 9.228 (±0.651), and it occurred at short times. Thus, increasing the CS content within the network increased the degree of swelling. This could be explained by the presence of more cationic moieties within the network at this pH level, thus the network expands more [38]. Similar polymeric interactions were observed in DSC patterns where shifts from the melting temperature peaks of polymers within IPCs at different times occurred.

To investigate the swelling kinetics of these systems, the parameters K_S and n were calculated by Eq. (3) [20]. It has been distinguished by three cases of diffusion according to the relative rates of diffusion and polymer relaxation. The first is Fickian diffusion ($n = 0.5$), in which the rate of diffusion is much less than the rate of relaxation. In this case, the system is controlled by diffusion. The second case is Case II ($n = 1.0$), where the diffusion process is much faster than the relaxation. The controlling step is the velocity of an advancing front, which forms the boundary between swollen hydrogel and glassy core. The third case is non-Fickian diffusion ($n = 0.5–1.0$), which describes those cases where the diffusion and relaxation rates are comparable.

The obtained results highlighted strong differences among complexes. The values of the exponent n were 0.736 (±0.010), 0.617 (±0.020), 0.402 (±0.030), 0.511 (±0.020) and 0.493 (±0.111), which correspond to CAM:[CS:CMC] 80:[90:10], 80:[75:25], 80:[50:50], 80:[25:75] and 80:[0:100] (w/w), respectively. They presented r^2 higher than 0.918 in all cases. The IPCs 80:[0:100], 80:[25:75] and 80:[50:50] (w/w) had n values close to 0.5, indicating Fickian water diffusion. However, the IPCs 80:[75:25] and 80:[90:10] had n ranged from 0.5 to 1, which indicated non-Fickian diffusion and diffusion–relaxation processes were involved.

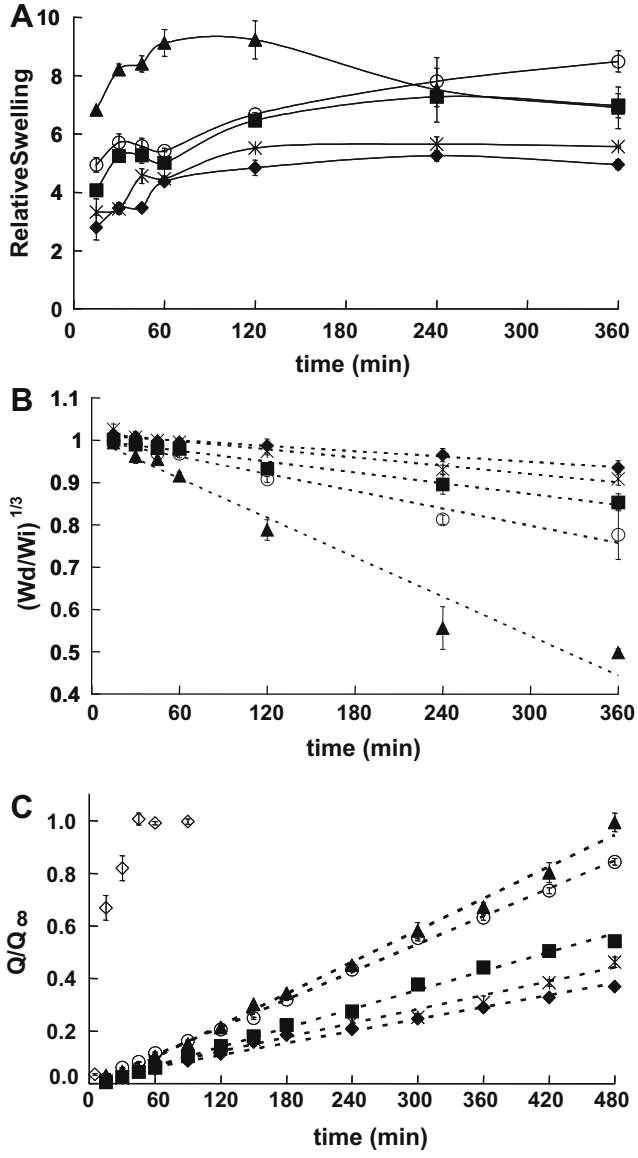

Fig. 10. *In vitro* relative swelling (A), erosion kinetics (B) and CAM release (C) at 37 °C and pH 4.2 of CAM:[CS:CMC] (w/w) 80:[100:0] (◇), 80:[90:10] (▲), 80:[75:25] (○), 80:[50:50] (■), 80:[25:75] (∗) and 80:[0:100] (♦), $n = 3$. Fitted experimental data to a linear equation (···).

In ionic cross-linked hydrogels, erosion of the network structure was prevented by ionic interactions that exist between both polymer chains. These labile bonds could be broken as a result of partial ionization of moieties that cause electrostatic repulsions [13].

Fig. 10B shows the eroding profiles of matrices comprised of CS and CMC, and their apparent polymer erosion rate constants were estimated.

All complexes present a linear behaviour with r^2 higher than 0.96 (data not shown), and the greatest erosion constant was observed in complexes with the highest content of CS. The values of the apparent polymer erosion constant (K_d) were 0.092 (±0.004), 0.040 (±0.008), 0.025 (±0.004), 0.019 (±0.001) and 0.015 (±0.003) h^{-1}, which correspond to CAM:[CS:CMC] 80:[90:10],

80:[75:25], 80:[50:50], 80:[25:75] and 80:[0:100] (w/w), respectively. Also, the erosion and release processes from IPCs were chemically confirmed with the microelemental measurements (data not shown). The C (%) content steadily decreased with time in acetate buffer. This fact could be explained by the presence of more ionized moieties within the network, and as a consequence, higher expansion between polymers and erosion rate. Similar results were obtained in others IPCs, where the greatest expansions of the network lead to the greatest erosions kinetics [15,34].

Furthermore, CAM is a barely water-soluble drug [7]; hence, it is expected that CAM release would be primarily controlled by erosion mechanisms.

3.5. In vitro drug release

Fig. 10C shows the release profiles obtained from hydrophilic matrices formulated with IPCs of CS and CMC.

The mini-matrices [CS:CMC] exhibited CAM-sustained release longer than 8 h, with the exception of CAM:[CS:CMC] 80:[100:0] (w/w) which all CAM was released at 45 min, so practically, it can be considered an immediate release. Within the IPCs, when increasing the content of CS, an increase in the drug release was observed. So, the fastest release was obtained from CAM:[CS:CMC] 80:[90:10] (w/w), which are in accordance with previous results obtained by FTIR. The low release of CAM at initial times (15 min) from matrices could be attributed to the low solubility of CAM at acidic media [7] and to the formation of a matrix system that was able to entrap efficiently the drug within the network [13,39].

These results are in accordance with the fact that the presence of more cationic moieties from CS which can be ionized and, consistently, major expansion of the systems and eroding process, because less pendants groups are involved in hydrogen bonding [12,38].

All profiles followed zero-order kinetics that could be corroborated by the good fit to a linear equation, with r^2 higher than 0.978. The values of the kinetic constants (K_o) were 0.201 (±0.007), 0.176 (±0.002), 0.120 (±0.002), 0.089 (±0.003) and 0.076 (±0.001) h^{-1}, which correspond to CAM:[CS:CMC] 80:[90:10], 80:[75:25], 80:[50:50], 80:[25:75] and 80:[0:100] (w/w), respectively. These kinetics could be related to the release profiles, meaning that the erosion process plays an important role in drug release. The prevalence of the erosion processes was expected, since CAM has a poor solubility at this pH level because it is a weak base with a pK_a of 8.76 [7].

4. Conclusions

Physicochemical characterization of all CS and CMC interpolymer complexes to form mini-matrices containing CAM have revealed polymer–polymer interactions. The data of XRD, FTIR and DSC demonstrated the formation of a new solvate of CAM when was placed in acetate buffer, as a result of crystallized molecules from solvent within its molecular structure.

During the tableting compression, matrix systems were formed, which was confirmed by DSC studies due to changes in the temperature of endothermic peaks of polymers.

The GID studies enabled us to profile the transformation of CAM on the surfaces of mini-matrices when it was in intimate contact with the dissolution medium, and its conversion to the solvate form prior to its dissolution process. Besides, DSC measurements have revealed polymer–polymer interactions and hydrogen bonding during dissolution process.

The swelling and eroding studies and *in vitro* drug release were carried out, and the results exhibited that when increasing the content of CS within the IPCs, swelling and erosion rates were greater and CAM release was faster at pH 4.2. This fact could be explained by the repulsion among $-NH_3^+$ from CS that results in a decrease in hydrogen bonds among carboxylic groups from CMC. However, at pH levels higher than CMC's pK_a (4.6), carboxylic moieties become ionized ($-COO^-$), which were responsible for an increased relative swelling in systems with high content of CMC.

The zero-order kinetics from release profiles were related to the linear behaviour of erosion kinetics, and highlighted that erosion process played an important role in drug release because CAM is poorly soluble in this medium.

Acknowledgements

This work was partially supported by a grant of the Complutense University and Madrid Community Administration to the research group 910939 (CCG07-UCM/BIO-2824) and by a grant of the Complutense University (PR1/08-15929-A). Also, M. Gómez-Burgaz has a pre-doctoral grant from the Complutense University of Madrid.

References

[1] Crystal Form 0 of Clarithromycin, US Patent 5,945,405, 1999.
[2] Processes for Preparing Clarithromycin Polymorphs and Novel Polymorph IV, Patent WO/2001/044262, 2001.
[3] Crystal Form I of Clarithromycin, Patent WO 98/004573, 1998.
[4] Preparation of Crystal Form II of Clarithromycin, Patent WO 98/004574, 1998.
[5] H. Suzuki, B.J. Marshall, T. Hibi, Overview: *Helicobacter pylori* and extragastric disease, Int. J. Hematol. 84 (2006) 291–300.
[6] Z. Liu, W. Lu, L. Qian, X. Zhang, P. Zeng, J. Pan, In vitro and in vivo studies on mucoadhesive microspheres of amoxicillin, J. Control. Release 102 (2005) 135–144.
[7] Y. Nakagawa, S. Itai, T. Yoshida, T. Nagai, Physicochemical properties and stability in the acidic solution of a new macrolide antibiotic, clarithromycin, in comparison with erythromycin, Chem. Pharm. Bull. 40 (1992) 725–728.
[8] S. Ramteke, N.K. Jain, Clarithromycin- and omeprazole-containing gliadin nanoparticles for the treatment of *Helicobacter pylori*, J. Drug. Target. 16 (2008) 65–72.
[9] J.K. Patel, M.M. Patel, Stomach specific anti-helicobacter pylori therapy: preparation and evaluation of amoxicillin-loaded chitosan mucoadhesive microspheres, Curr. Drug Deliv. 4 (2007) 41–50.
[10] J. Berger, M. Reist, J.M. Mayer, O. Felt, N.A. Peppas, R. Gurny, Structure and interactions in covalently and ionically crosslinked chitosan hydrogels for biomedical applications, Eur. J. Pharm. Biopharm. 57 (2004) 19–34.
[11] E.K. Just, T.G. Majewicz, Encyclopedia of Polymer Science and Engineering, vol. 3, John Wiley and Sons, New York, 1985, p. 226.
[12] G.A. Abdelbary, M.I. Tadros, Design and in vitro/in vivo evaluation of a novel nicorandil extended release matrix tablets based on hydrophilic interpolymer complexes and a hydrophobic waxy polymer, Eur. J. Pharm. Biopharm. 69 (2008) 1019–1028.
[13] P.M. de la Torre, Y. Enobakhare, G. Torrado, S. Torrado, Release of amoxicillin from polyionic complexes of chitosan and poly(acrylic acid). Study of polymer/polymer and polymer/drug interactions within the network structure, Biomaterials 24 (2003) 1499–1506.
[14] S.K. Motwani, S. Chopra, S. Talegaonkar, K. Kohli, F.J. Ahmad, R.K. Khar, Chitosan–sodium alginate nanoparticles as submicroscopic reservoirs for ocular delivery: formulation, optimisation and in vitro characterization, Eur. J. Pharm. Biopharm. 68 (2008) 513–525.
[15] F. Chellat, M. Tabrizian, S. Dimitriu, E. Chornet, C.H. Rivard, L. Yahia, Study of biodegradation behaviour of chitosan-xanthan microspheres in simulated physiological media, J. Biomed. Mater. Res. 53 (2000) 592–599.
[16] Y.H. Li, J.B. Zhu, Modulation of combined-release behaviors from a novel "tablets-in-capsule system", J. Control. Release 95 (2004) 381–389.
[17] M. Koivisto, P. Heinanen, V.P. Tanninen, V.-P. Lehto, Depth profiling of compression-induced disorders and polymorphic on tablet surfaces with grazing incidence X-ray diffraction, Pharm. Res. 23 (2006) 813–820.
[18] C.A.M. Stedman, M.L. Barclay, Review article: comparison of the pharmacokinetics, acid suppression and efficacy of proton pump inhibitors, Aliment. Pharmacol. Ther. 14 (2000) 963–978.
[19] N. Kavanagh, O.I. Corrigan, Swelling and erosion properties of hydroxypropylmethylcellulose (Hypromellose) matrices – influence of agitation rate and dissolution medium composition, Int. J. Pharm. 279 (2004) 141–152.
[20] G.W.R. Davidson III, N.A. Peppas, Relaxation-controlled transport in P(HEMA-co-MMA) copolymers, J. Control. Release 3 (1986) 243–258.
[21] S. Debnath, P. Predecki, R. Suryanarayanan, Use of glancing angle X-ray powder diffractometry to depth-profile phase transformations during dissolution of indomethacin and theophylline tablets, Pharm. Res. 21 (2004) 149–159.
[22] Y. Inoue, S. Yoshimura, Y. Tozuka, K. Moribe, T. Kumamoto, T. Ishikawa, K. Yamamoto, Application of ascorbic acid 2-glucoside as a solubilizing agent for

clarithromycin: solubilization and nanoparticle formation, Int. J. Pharm. 331 (2007) 38–45.
[23] Y.-T. Sohn, J.-K. Rhee, W.-B. Im, Polymorphism of clarithromycin, Arch. Pharm. Res. 23 (2000) 381–384.
[24] A. Ghaffari, K. Navaee, M. Oskoui, K. Bayati, M. Rafiee-Tehrani, Preparation and characterization of free mixed-film of pectin/chitosan/Eudragit RS intended for sigmoidal drug delivery, Eur. J. Pharm. Biopharm. 67 (2007) 175–186.
[25] S. Puttipipatkhachorn, J. Nunthanid, K. Yamamoto, G.E. Peck, Drug physical state and drug–polymer interaction on drug release from chitosan matrix films, J. Control. Release 75 (2001) 143–153.
[26] J. Aaltonen, P. Heinänen, L. Peltonen, H. Kortejärvi, V.P. Tanninen, L. Christiansen, J. Hirvonen, J. Yliruusi, J. Rantanen, In situ measurement of solvent-mediated phase transformations during dissolution testing, J. Pharm. Sci. 95 (2006) 2730–2737.
[27] M.R. Caira, G. Bettinetti, M. Sorrenti, L. Catenacci, Relationship between structural and thermal properties of anhydrous and solvated crystalline forms of brodimoprim, J. Pharm. Sci. 96 (2007) 996–1007.
[28] A. Othman, J.S.O. Evans, I.R. Evans, R.K. Harris, P. Hodgkinson, Structural study of polymorphs and solvates of finasteride, J. Pharm. Sci. 96 (2007) 1380–1397.
[29] R. Henry, G.G.Z. Zhang, Crystallographic characterization of several erythromycin A solvates: the environment of the solvent molecules in the crystal lattice, J. Pharm. Sci. 96 (2007) 1251–1257.
[30] C.-Y. Lii, P. Tomasik, H. Zaleska, S.-C. Liaw, V.M.-F. Lai, Carboxymethylcellulosegelatin complexes, Carbohyd. Polym. 50 (2002) 19–26.
[31] G. Pasparakis, N. Bouropoulos, Swelling studies and in vitro release of verapamil from calcium alginate and calcium alginate–chitosan beads, Int. J. Pharm. 323 (2006) 34–42.
[32] S.-M. Cho, H.-K. Choi, Preparation of mucoadhesive chitosan-poly(acrylic acid) microspheres by interpolymer complexation and solvent evaporation method I, Int. J. Kor. Pharm. Sci. 35 (2005) 95–99.
[33] C.G.T. Neto, J.A. Giacometti, A.E. Job, F.C. Ferreira, J.L.C. Fonseca, M.R. Pereira, Thermal analysis of chitosan based networks, Carbohyd. Polym. 62 (2005) 97–103.
[34] Y. Javadzadeh, L. Musaalrezaei, A. Nokhodchi, Liquisolid technique as a new approach to sustain propanolol hydrochloride release from tablet matrices, Int. J. Pharm. 362 (2008) 102–108.
[35] G.A. Gonzalez Novoa, J. Heinämäki, S. Mirza, O. Antikainen, A.I. Colarte, A.S. Paz, J. Yliruusi, Physical solid-state properties and dissolution of sustained-release matrices of polyvinylacetate, Eur. J. Pharm. Biopharm. 59 (2005) 343–350.
[36] J. Ma, Y. Xu, B. fan, B. Liang, Preparation and characterization of sodiummethylcellulose/poly(*N*-isopropylacrylamide)/clay semi-IPN nanocomposite hydrogels, Eur. Polym. J. 43 (2007) 2221–2228.
[37] M. Cooney, J. Petermann, C. Lau, S. Minteer, Characterization evaluation of hydrophobically modified chitosan scaffolds: towards design of enzyme immobilized flow-through electrodes, Carbohyd. Polym. 75 (2009) 428–435.
[38] K. Mladenovska, R.S. Raicki, E.I. Janevik, T. Ristoski, M.J. Pavlova, Z. Kavrakovski, M.G. Dodov, K. Goracinova, Colon-specific delivery of 5-aminosalicylic acid from chitosan–Ca–alginate microparticles, Int. J. Pharm. 342 (2007) 124–136.
[39] P. Lim Soo, J. Cho, J. Grant, E. Ho, M. Piquette-Miller, C. Allen, Drug release mechanism of paclitaxel from a chitosan–lipid implant system: effect of swelling degradation and morphology, Eur. J. Pharm. Biopharm. (2008), doi:10.1016/j.ejpb.2007.11.003.